Improved Carbon and Nitrogen Isotopic Ratios for CH3CN in Titan's Atmosphere Using ALMA

Nosowitz Jonathon, M A Cordiner, C A Nixon, A E Thelen, Zbigniew Kisiel, N A Teanby, Patrick G. J. Irwin, Steven B Charnley, Véronique Vuitton

Draft version October 3, 2024
Typeset using LaTeX **twocolumn** style in AASTeX631

Improved Carbon and Nitrogen Isotopic Ratios for CH_3CN in Titan's Atmosphere Using ALMA

Jonathon Nosowitz [1,2] Martin A. Cordiner [2,1] Conor A. Nixon [2] Alexander E. Thelen [3] Zbigniew Kisiel [4] Nicholas A. Teanby [5] Patrick G. J. Irwin [6] Steven B. Charnley [2] and Véronique Vuitton [7]

[1] *Department of Physics, The Catholic University of America, Washington, DC 20064, USA*
[2] *Solar System Exploration Division, NASA Goddard Space Flight Center, Greenbelt, MD 20771, USA*
[3] *Division of Geological and Planetary Sciences, California Institute of Technology, Pasadena, CA 91125, USA*
[4] *Institute of Physics, Polish Academy of Sciences, Al. Lotników 32/46, 02-668 Warszawa, Poland*
[5] *School of Earth Sciences, University of Bristol, Bristol BS8 1RJ, UK*
[6] *Atmospheric, Oceanic and Planetary Physics, Clarendon Laboratory, University of Oxford, Oxford OX1 3PU, UK*
[7] *Univ. Grenoble Alpes, CNRS, IPAG, 38000 Grenoble, France*

ABSTRACT

Titan, Saturn's largest satellite, maintains an atmosphere composed primarily of nitrogen (N_2) and methane (CH_4) that creates complex chemistry. Within this complex chemistry exist nitrile (or cyanide) molecules that have a -CN group. These molecules are known to have substantially enhanced ^{15}N abundances compared to Earth and Titan's dominant nitrogen (N_2) reservoir. The $^{14}N/^{15}N$ isotopic ratio in Titan's nitriles can provide better constraints on the synthesis of nitrogen-bearing organics in planetary atmospheres as well as the origin of Titan's large nitrogen abundance. Using high signal-to-noise, disk-integrated observations obtained with the Atacama Large Millimeter/submillimeter Array (ALMA) Band 6 receiver (211-275 GHz), we determine the $^{14}N/^{15}N$ and $^{12}C/^{13}C$ isotopic ratios of acetonitrile (CH_3CN) in Titan's stratosphere. Using the Nonlinear optimal Estimator for MultivariatE spectral analySIS (NEMESIS), we derived the $CH_3CN/^{13}CH_3CN$ ratio to be 89.2 ± 7.0 and the $CH_3CN/CH_3{}^{13}CN$ ratio to be 91.2 ± 6.0, in agreement with the $^{12}C/^{13}C$ ratio in Titan's methane, and other Solar System materials. We found the $^{14}N/^{15}N$ isotopic ratio to be 68.9 ± 4.2, consistent with previously derived values for HCN and HC_3N, demonstrating an enhanced ^{15}N abundance in Titan's nitriles compared with the bulk atmospheric N_2 value of $^{14}N/^{15}N = 168$ suggesting a significant role of fractionation in Titan's nitrogen chemistry.

Keywords: Titan — Remote Sensing — Radio/sub-mm interferometry — Atmospheric Chemistry

1. INTRODUCTION

The origin and evolution of the atmosphere of Titan, Saturn's largest satellite, has been an area of interest for many years. Titan's atmosphere is substantial and has intricate chemistry for a moon and can help elucidate the compositions of primitive (exo-)planetary atmospheres. As we continue to investigate Titan's atmosphere more questions arise on topics such as cloud and haze formation, chemical pathways, interactions with surface and sub-surface features, as well as others (Nixon et al. 2018; MacKenzie et al. 2021), so some of the critical information needed to eliminate the gaps in our knowledge continues to elude us. We know that Titan maintains a thick atmosphere that is composed primarily of molecular nitrogen (N_2) at about 98% and methane (CH_4) at about 2%. But the source of these molecules, particularly that of N_2, is not well known. Glein (2015) suggests that the gases that formed Titan's atmosphere were trapped in its core and that hydrothermal and cryovolcanic process were critical to the formation of Titan's atmosphere. However, this is reliant on chemical reactions, outgassing, and transport mechanisms to produce the gas abundances that are currently measured in Titan's atmosphere. Glein (2015) shows that this method is plausible through mass balance and chemical equilibrium calculations, but also acknowledges that miss-

Corresponding author: Jonathon Nosowitz
nosowitz@cua.edu

ing information, such as a value for a reasonable outgassing efficiency, makes it challenging to conclusively validate the theory. Thus, for molecules like N_2, Glein (2015) suggests looking at the nitrogen isotopic ratio of cometary gases as the source of Titan's N_2. The ratios derived from cometary gases are similar to those of Titan's atmosphere suggesting that the primordial NH_3 reservoir represented by cometary ices could be the source of Titan's nitrogen (Mandt et al. 2014).

The N_2 and CH_4 in Titan's atmosphere form the basis of a complex chemical reaction network, yet the chemistry involving nitrogen is still not fully constrained (Hörst 2017; Nixon 2024). It is particularly important to understand the chemistry of nitriles (or cyanides; molecules that have a -CN group), due to their large atmospheric abundances, as well as their possible role in prebiotic syntheses (Oro et al. 1990).

Nitriles often possess a large dipole moment, and thus their rotational transitions can be detected in Titan's atmosphere at mm/sub-mm wavelengths, including HCN, HC_3N, CH_3C_3N, C_2H_5CN and more (Hörst 2017; Nixon et al. 2020; Cordiner et al. 2015; Palmer et al. 2017; Thelen et al. 2020). These molecules, and a diverse population of other organics, are generated in Titan's upper atmosphere through high-altitude photochemistry, following dissociation by UV photons, and collisions with charged particles from Saturn's magnetosphere, or galactic cosmic rays.

Previously-developed photochemical models (*e.g.* (Dobrijevic & Loison 2018; Vuitton et al. 2019; Wilson & Atreya 2004; Willacy et al. 2016)) obtain a moderately good agreement with the observed abundances of many nitrogen-bearing species in Titan's atmosphere, suggesting good progress in our quantitative understanding of the relevant chemical processes. However, there still exist significant gaps in our knowledge of Titan's photochemistry. The available photochemical models make different assumptions regarding the relevant reaction pathways, and the $^{14}N/^{15}N$ ratios in Titan's nitriles are particularly sensitive to some of these assumptions. Enrichment (or isotopic fractionation) of ^{15}N relative to Titan's bulk N_2 reservoir is theorized to occur as a result of isotope selective photodissociation of N_2 at high altitudes, leading to a reservoir of gas-phase atomic nitrogen that is isotopically enriched in ^{15}N. The resulting ^{15}N enrichment is readily passed on to nitrogen-bearing photochemical products. However, the atomic $^{14}N/^{15}N$ ratio is observationally unconstrained, and is sensitive to the various model parameters. Incorporation of ^{15}N into nitriles occurs at different rates depending on the altitude-dependent reaction pathways; indeed, the $^{14}N/^{15}N$ isotopic ratio in CH_3CN has been shown to depend on the relative efficiencies of the different formation pathways (Dobrijevic & Loison 2018), which are not yet fully constrained by experiments. Further studies of the $^{14}N/^{15}N$ ratios in Titan's nitriles are therefore needed, to improve our understanding of the relevant chemical processes, leading to a better understanding of nitrogen chemistry (including isotope chemistry) in planetary atmospheres.

The first $^{14}N/^{15}N$ isotopic ratio measurement of Titan's atmosphere was by Marten et al. (2002), who used the Institut de Radioastronomie Millimétrique (IRAM) 30-m telescope to derive a value of $HC^{14}N/HC^{15}N = 60$–70 in the stratosphere. Another measurement of HCN was made by Cassini in the infrared (Vinatier et al. 2007) with a derived $^{14}N/^{15}N$ ratio of 56 ± 8. The $HC^{14}N/HC^{15}N$ ratio was further refined by Molter et al. (2016) who obtained a value of 72.2 ± 2.2 using high spectral-resolution ALMA data. Cassini obtained in-situ $^{14}N_2/^{15}N^{14}N$ measurements, from which an isotopic ratio of 167.7 ± 0.6 was derived in N_2, which represents the dominant atmospheric nitrogen reservoir (Niemann et al. 2010). More recently, Cordiner et al. (2018) and Iino et al. (2020) used ALMA to obtain $^{14}N/^{15}N$ ratios of 67 ± 14 and 125^{+145}_{-44} in HC_3N and CH_3CN, respectively. The difference in ^{15}N fractions between the (trace) photochemical products and the (bulk) nitrogen reservoir can be explained as a result of isotope selective N_2 photodissociation by solar radiation (Liang et al. 2007), but the significance of any differences in the degree of ^{15}N enrichment among different nitriles is yet to be investigated in detail. As one of the most abundant nitriles in Titan's atmosphere, more accurate measurements of the CH_3CN istopologues, in particular, are justified, to help test and improve models for Titan's nitrogen chemistry.

2. OBSERVATIONS

To investigate Titan's high-altitude nitrogen chemistry, we obtained observations using the Atacama Large Millimeter/submillimeter Array (ALMA) band 6 receiver (211-275 GHz; ∼1.1-1.4 mm), in 2019 as part of project #2019.1.00783.S. Three spectral settings were observed, two of which included observations of multiple nitrile species and their carbon and nitrogen isotopes.

As described by Thelen et al. (2020), the data were taken during multiple execution blocks between November 14 and December 16, 2019 using ALMA configurations C43-1, C43-2 (maximum baselines ranging from 160 to 314 m), and C43-3 (maximum baselines of 500 m). The resulting beam size was $1.54''$x$1.14''$ in the 256-257 GHz range and in the 267-268 GHz range, so Titan ($\approx 1.0''$ on the sky, including its solid disk and extended atmosphere) was not resolved, enabling the maximum sensitivity per beam for disk-averaged studies of Titan's

entire Earth-facing atmosphere. The spectral resolution of the CH_3CN and $CH_3{}^{13}CN$ isotopologues was 488 kHz and the resolution for the $^{13}CH_3CN$ and $CH_3C^{15}N$ isotopologues was 976 kHz. The data were processed and calibrated using version 5.6.1-8 of the Common Astronomy Software Applications (CASA) pipeline using standard scripts provided by the Joint ALMA Observatory (JAO). Additional bandpass calibration smoothing was performed, to improve the spectral noise per channel, and the `tclean` procedure was used to reconstruct the sky model. For a more complete description of the observations and data processing, we refer the reader to Thelen et al. (2020).

A list of the observed CH_3CN spectral lines of relevance to the present study, their frequencies and upper state energies (E_u) are shown in Table 1.

3. RADIATIVE TRANSFER MODELING

From the processed data cubes, disk-averaged spectra were extracted using a circular aperture with radius of 1.8″, which was divided up into 35 annuli corresponding to different emission angles, in the range of 3-75 degrees, with respect to the top of Titan's atmosphere (Teanby et al. 2013). The model was extended from the surface to 1200 km. Spectral models were generated using the line-by-line module of the Nonlinear optimal Estimator for MultivariatE spectral analySIS (NEMESIS) radiative transfer and retrieval tool (Irwin et al. 2008). NEMESIS applies an iterative minimization technique to the cost function (including the goodness of fit, χ^2) in order to obtain an optimized spectral model and vertical abundance and temperature profiles as a function of altitude. NEMESIS includes the necessary physical parameters such as spontaneous emission and absorption of radiation, on and off-limb emission angles, continuum opacity and thermal and pressure broadening, as well as temperature dependence when computing model fluxes as a function of wavelength. This allows a full characterization of the observed spectral line profiles, leading to robust abundance measurements.

To further ensure highest accuracy of our model retrieval results, updates were made to the spectral line database and instrumental broadening function. The NEMESIS line database was updated to the GEISA 211 format for additional precision on the rest frequencies and intensities. We initially used the line data from The Cologne Database for Molecular Spectroscopy (Müller et al. 2001) but found discrepancies in the line intensities and partition function coefficients for the major isotopologue and ^{13}C minor isotopologues. All of the values were re-computed without hyperfine or vibrational corrections in a self-consistent manner. Note that the hyperfine splittings for all relevant transitions are much smaller than the resolution of our observed spectra. We refer the reader to Appendix A for more details. The partition functions for all of the isotopologues were tabulated for inclusion in NEMESIS using a fourth order polynomial fit to the re-computed values listed in Table 2. We also updated the instrumental line shape used by NEMESIS, to account for the intrinsic (non-Gaussian) shape of the ALMA line spread function, as well as including the potential effects of rotational broadening of the lines due to Titan's zonal winds (see Appendix B for details).

Optimization of the vertical abundance profile began with a reasonable guess based on prior measurements. For the major CH_3CN isotopologue, we used an a priori profile based on the disk-averaged measurements from Marten et al. (2002) up to 500 km, supplemented by data from the model of Loison et al. (2015) up to 1200 km. The error on the profile was kept constant at 100%. From the N_2 broadening parameters of CH_3CN calcu-

Table 1. Observed CH_3CN isotopologue transitions

Species	Transition[a]	Rest. Freq. (GHz)	E_u (K)
CH_3CN	14_6-13_6	257.3491793	349.7
CH_3CN	14_5-13_5	257.4035843	271.2
CH_3CN	14_4-13_4	257.4481277	206.9
CH_3CN	14_3-13_3	257.4827915	156.9
CH_3CN	14_2-13_2	257.5075614	121.2
CH_3CN	14_1-13_1	257.5224275	99.8
CH_3CN	14_0-13_0	257.5273835	92.7
$CH_3{}^{13}CN$	14_3-13_3	257.3555752	156.9
$CH_3{}^{13}CN$	14_2-13_2	257.3802430	121.2
$CH_3{}^{13}CN$	14_1-13_1	257.3950476	99.8
$CH_3{}^{13}CN$	14_0-13_0	257.3999832	92.6
$CH_3C^{15}N$	15_5-14_5	267.4868839	281.6
$CH_3C^{15}N$	15_4-14_4	267.5323198	217.2
$CH_3C^{15}N$	15_3-14_3	267.5676777	167.1
$CH_3C^{15}N$	15_2-14_2	267.5929435	131.3
$CH_3C^{15}N$	15_1-14_1	267.6081070	109.9
$CH_3C^{15}N$	15_0-14_0	267.6131621	102.7
$^{13}CH_3CN$	15_5-14_5	267.8245852	281.7
$^{13}CH_3CN$	15_4-14_4	267.8698337	217.3
$^{13}CH_3CN$	15_3-14_3	267.9050464	167.2
$^{13}CH_3CN$	15_2-14_2	267.9302086	131.5
$^{13}CH_3CN$	15_1-14_1	267.9453102	110.0
$^{13}CH_3CN$	15_0-14_0	267.9503447	102.8

[a] Rotational transitions are denoted as J_K-J_K where the transition is from the upper state to the lower state and K represents the angular momentum quantum number

lated by Dudaryonok et al. (2015), we assumed an average value for the Lorentzian half-width using the K=0 & K=5 J=14-13 coefficients (Γ = 0.158 cm^{-1} atm^{-1}) and temperature exponent (α = 0.60). A temperature profile using the data from Thelen et al. (2020) was used as an a priori profile, with errors kept small enough so that the profile did not need to be re-retrieved. A correlation length of 3.0 atmospheric scale heights was used to internally smooth the optimized profiles. The CH_3CN major isotopologue and temperature profiles were continuously retrieved simultaneously at each altitude to improve the fit to the main CH_3CN lines.

The minor CH_3CN isotopologue spectra are noisier and contain less vertical information, so we used the best-fitting CH_3CN main isotope abundance profile scaled by a uniform factor, which was varied to obtain the best fit. The results of an attempted, continuously-variable $CH_3C^{15}N$ retrieval, are discussed in Appendix C.

4. RESULTS

Our CH_3CN spectral fits and retrieved vertical abundance and temperature profiles are shown in Figure 1. We derived scaling factors representative of the mean isotopic ratios over Titan's disk-averaged atmosphere, for the three CH_3CN isotopologues, including the ^{15}N isotopologue and both ^{13}C isotopologues. The $CH_3CN/CH_3C^{15}N$ isotopic ratio was derived to be 68.9 $\pm$ 4.2, the $CH_3CN/^{13}CH_3CN$ ratio was derived to be 89.2 $\pm$ 7.0, and the $CH_3CN/CH_3{}^{13}CN$ ratio was derived to be 91.2 $\pm$ 6.0. Our derived $^{14}N/^{15}N$ isotopic ratio for the major isotopologue is shown for comparison with previously obtained ratios for HCN, HC_3N and CH_3CN as well as N_2 in Figure 2.

Within the noise, our spectral models provide an excellent fit to the observed Titan continuum, line cores and line wings.

In the lower stratosphere (below 150 km altitude), our retrieved CH_3CN vertical abundance (VMR) profile matches closely the steepness of the Marten et al. (2002) a-priori. Our retrieved abundances drop somewhat below the a-priori in the mid-to-upper stratosphere, with the notable exception of a bump around 250 km, although there may be some doubt as to the physical origin of this relatively narrow feature, since it is not present in the ALMA profile retrieved by Lellouch et al. (2019), or the photochemical model results of Vuitton et al. (2019); Dobrijevic & Loison (2018). Considering our observations are averaged over Titan's entire Earth-facing hemisphere, the resulting spectra represent a weighted average across all latitudes and altitudes. It therefore cannot be determined where exactly (latitudinally) in Titan's atmosphere this bump originates. On the other hand, this feature is found to be necessary to obtain a good fit to the observed spectra — otherwise, the line core and wing strengths cannot be simultaneously reproduced.

Based on the CH_3CN maps previously published by Thelen et al. (2019, 2024) and Cordiner et al. (2019), CH_3CN is most concentrated around Titan's poles. The stratospheric CH_3CN enhancement could be consistent with the presence of an unresolved abundance peak(s) within the beam, associated with one or both of these regions. It can be speculated that the contribution is potentially coming from the trapping of molecules and subsidence in the (cold) polar regions, possibly at different altitudes around the north and south poles (see Teanby et al. (2008, 2017, 2019), for example).

We then used the contribution functions from our best-fitting radiative transfer models to calculate weighted mean emission altitudes, which represent the average altitude to which our results are sensitive. These were determined to be ~246 km for the major isotopologue and ~230 km for the $^{13}CH_3CN$ and $CH_3C^{15}N$ isotopologues.

To make a detailed comparison with the $CH_3CN/CH_3C^{15}N$ vertical profiles produced by photochemical models, we also performed a continuously-variable $CH_3C^{15}N$ VMR fit. However, the spectroscopic signal-to-noise ratio was found to be insufficient to properly constrain the $^{14}N/^{15}N$ ratio as a function of altitude (see Appendix C).

5. DISCUSSION

We now compare our isotopic ratios to those previously obtained in the Titan literature. We find that our $CH_3CN/CH_3C^{15}N$ ratio of 68.9 $\pm$ 4.2 is significantly lower than the $^{14}N/^{15}N$ ratio in N_2 of 167.7 $\pm$ 0.6 obtained by Cassini mass spectrometry (Niemann et al. 2010), indicating strong ^{15}N enrichment in Titan's CH_3CN. On the other hand, our result is within 1.6-σ of the previous Cassini CIRS measurement for HCN (56 $\pm$ 8; Vinatier et al. 2007), and is within 1-σ of the HCN measurement using ALMA (72.2 $\pm$ 2.2; Molter et al. 2016). Within the errors, our result is also consistent with the $^{14}N/^{15}N$ ratio in HC_3N (67 $\pm$ 14; Cordiner et al. 2018), and within 1.3-σ of the previous best value for the $CH_3CN/CH_3C^{15}N$ ratio of 125^{+145}_{-44}, obtained using ALMA archival flux calibration data by Iino et al. (2020). Although the apparent difference between our value and that of Iino et al. (2020) could be explained solely as a result of statistical noise, it should be noted that our improved values for the spectral line intensities and partition functions compared with those

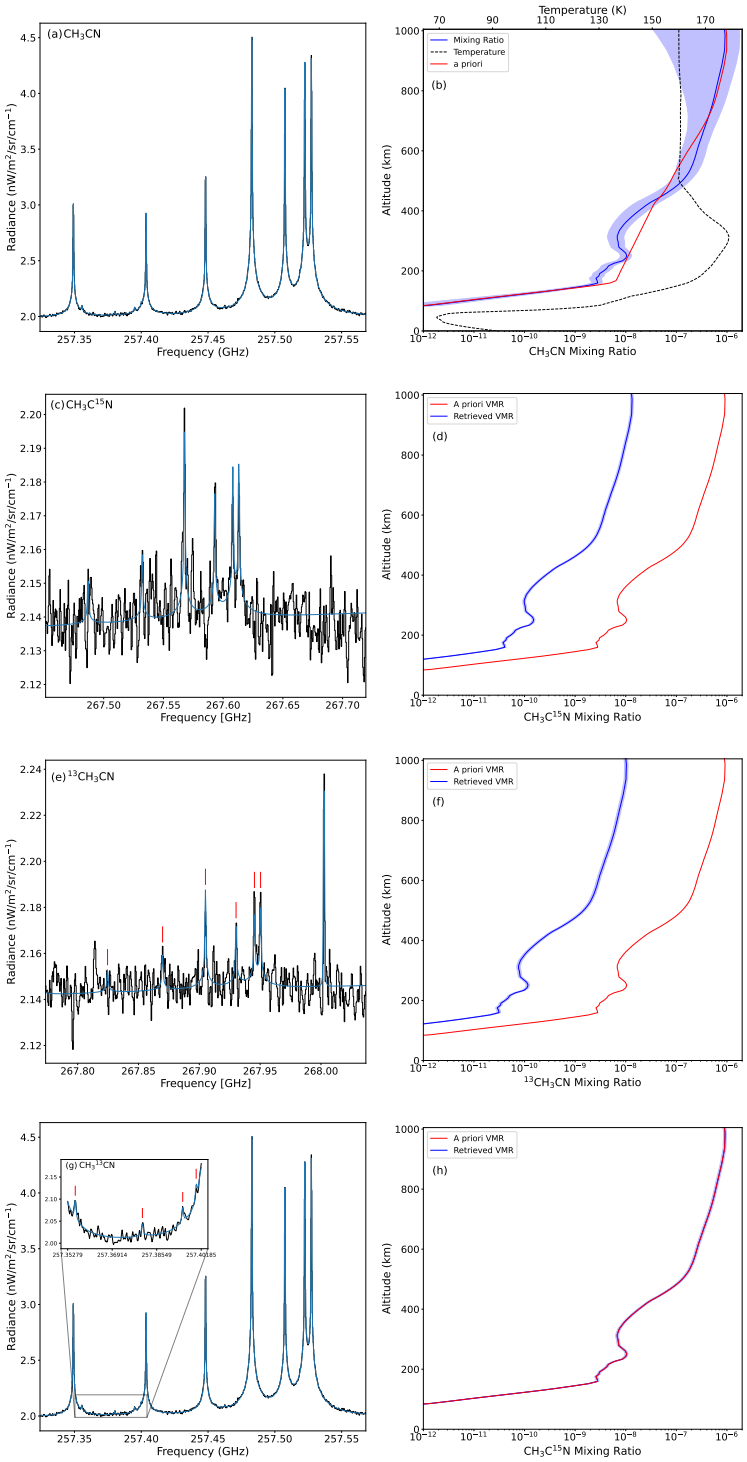

Figure 1. Optimized model fits for all isotopologues in the left column. The data is in black and the model is in blue. The molecule is identified in the top left corner of the panel. The respective retrieved vertical profiles (volume mixing ratios or VMRs) are in the right column. In all profiles, the red line is the a priori profile, the blue line is the retrieved VMR profile and the shaded region is error on the retrieved VMR profile. For the major isotopologue, the dashed black line is the continuously retrieved temperature profile. The error envelope of the minor isotopologues is quite narrow, it is within 6-8% of the obtained isotope ratio value. The red ticks in (e) and (g) identify the $^{13}CH_3CN$ and $CH_3{}^{13}CN$ lines, respectively, in the data. The highest frequency line in (e) is the J=30-29 K_a=3 transition of C_2H_5CN (propionitrile; ethyl cyanide) at 268.0025 GHz. Following the order of the plots above, the χ^2_ν for the isotopologues are 1.01, 0.9380, 1.02, 1.02. We used the residuals of the pseudo-continuum, regions of the spectrum that don't include contributions from line cores, to calculate the χ^2_ν and took into account the correlation length of 3.0 atmospheric scale heights to calculate the number of free parameters.

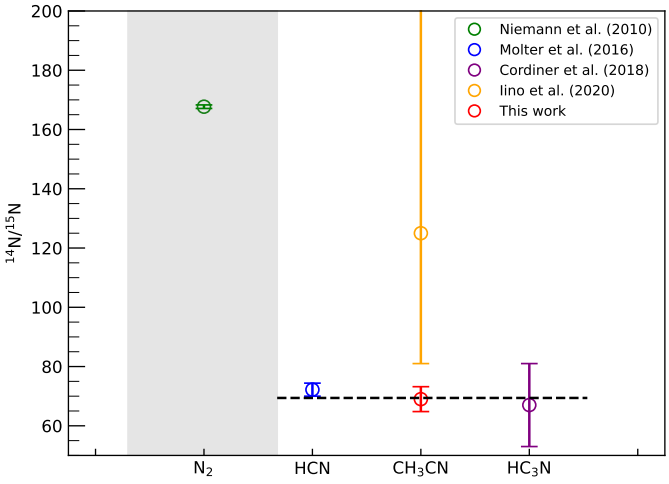

Figure 2. Previously derived $^{14}N/^{15}N$ isotopic ratios for molecules in Titan's atmosphere, including the value derived in this work in red. The N_2 data point is plotted against a gray background to distinguish it as the main atmospheric nitrogen reservoir. The black dashed line is the average of our CH_3CN value and the HCN and HC_3N values from Molter et al. (2016) and Cordiner et al. (2018), respectively.

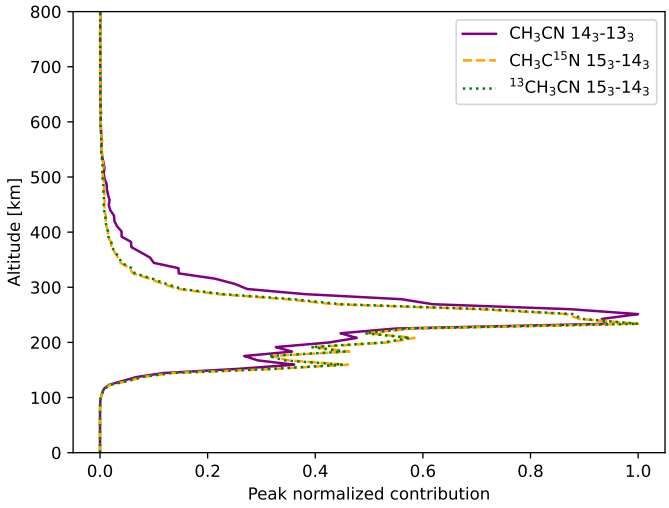

Figure 3. Cross-section view of the contribution functions for the strongest lines (K=3) of CH_3CN and its minor isotopologues.

in the CDMS database (see Appendix A) resulted in a downward revision of the $^{14}N/^{15}N$ ratio by ∼18% and $^{12}C/^{13}C$ ratio by ∼23% for the $CH_3CN/^{13}CH_3CN$ ratio and by ∼34% for the $CH_3CN/CH_3{}^{13}CN$ ratio, to obtain our final results, so this could explain some of the discrepancy.

Overall, our derived ratio is in relatively good agreement with the previously obtained ratios with the exception of N_2. By far the dominant form of nitrogen in Titan's atmosphere is N_2, so we take the $^{14}N/^{15}N$ ratio in N_2 to be representative of Titan's intrinsic isotopic composition. Isotope-selective photodissociation of N_2 in the upper atmosphere provides a reservoir of ^{15}N-enriched atomic nitrogen that feeds into the altitude dependent nitrogen chemistry, resulting in the synthesis of ^{15}N-enriched nitriles such as CH_3CN. In Figure 57 of Vuitton et al. (2019), the peak density for atomic ^{14}N and ^{15}N occurs in Titan's thermosphere between 1100-1200 km, falling rapidly below ∼700 km. However, the atomic $^{15}N/^{14}N$ isotopic ratio reaches a peak value of ∼0.04 at ∼900 km, below the point of the peak atomic ^{14}N and ^{15}N values. There are approximately constant values for the wings of the distribution of the $^{15}N/^{14}N$ ratio: ∼0.015 at ∼1200 km and above and ∼0.005 at ∼800 km and below. Thus, the incorporation of fractionated nitrogen, and therefore production of nitriles, occurs above ∼700 km, followed by downward mixing and diffusion toward the stratosphere, into the region between 150-300 km, to which our ALMA observations are most sensitive. The enriched ^{15}N abundance in the main nitrile production thus leads to a decrease in the $^{14}N/^{15}N$ isotopic ratio for CH_3CN. The large difference between the isotopic ratios in N_2 and CH_3CN is consistent with this picture. Also comparing the $^{14}N/^{15}N$ ratio profiles for HCN, CH_3CN and HC_3N shown in Figure 58 of Vuitton et al. (2019) reveals that they should be expected to follow a similar general trend, with decreased values at altitudes below ∼800 km.

Isotopic ratios for $^{12}C/^{13}C$ have previously been measured on Titan for CH_4 (Niemann et al. 2010), CO_2 (Nixon et al. 2008b), ^{13}CO (Serigano et al. 2016), C_4H_2 (Jolly et al. 2010), C_2H_2 (Nixon et al. 2008a), C_2H_6 (Nixon et al. 2008a), HC_3N (Jennings et al. 2008), and HCN (Molter et al. 2016). Comparing the error weighted mean isotopic ratio for these molecules, 89.9 ± 1.4, to our derived $^{12}C/^{13}C$ ratios in CH_3CN of 89.2 ± 7.0 and 91.2 ± 6.0, we find that they are all consistently within a 1-σ error margin. Additionally, when comparing our derived $^{12}C/^{13}C$ ratios to the error-weighted mean for comets (88.6 ± 6.5, which excludes the outlier for H_2CO in comet 67P; Altwegg et al. 2020), and with the terrestrial value of 89.0, we also find that our measurements are within 1-σ. Thus, our $^{12}C/^{13}C$ ratios are also in good agreement with the values previously derived for Titan and various other Solar System materials, including other bodies within the Saturnian system (see Nomura et al. 2022, and references therein).

The improved accuracy of our $CH_3CN/CH_3C^{15}N$ ratio compared with Iino et al. (2020) leads to new constraints on models for the CH_3CN production pathways and nitrogen fractionation processes in Titan's atmo-

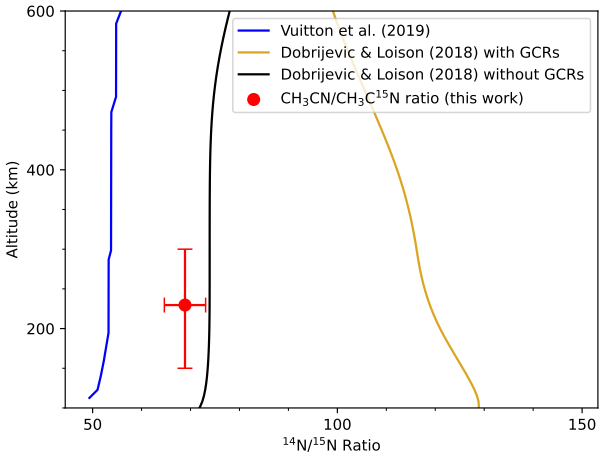

Figure 4. Our derived scaling factor for the $CH_3CN/CH_3C^{15}N$ isotopic ratio (red point) with horizontal error bars showing the error on the ratio value and the vertical bars spanning the region of highest sensitivity, 150-300 km, with the ratio profiles from the Vuitton et al. (2019) (blue line) and Dobrijevic & Loison (2018) photochemical models (black (without GCRs) and gold (with GCRs)).

sphere. The model by Vuitton et al. (2019) includes multiple pathways to CH_3CN, the most important being

$$H + CH_2CN \xrightarrow{M} CH_3CN \quad (1)$$

$$N(^2D) + C_2H_4 \longrightarrow CH_3CN + H \quad (2)$$

and

$$HCNH^+ + CH_3 \longrightarrow CH_3CNH^+ \quad (3)$$

followed by

$$CH_3CNH^+ + e^- \longrightarrow CH_3CN + H \quad (4)$$

Balucani et al. (2012) showed that equation 2, is inefficient since it favors the alternative isomeric product forms — CH_2NCH and c-$CH_2(N)CH$ — rather than CH_3CN. Dobrijevic & Loison (2018) suggested that equation 1 may not be the dominant route to CH_3CN since it primarily occurs at the higher pressures found in the lower atmosphere.

If reaction 3 is the primary route to CH_3CN (and therefore $CH_3C^{15}N$ via $HC^{15}NH^+$), then this could help explain the similarity between the observed $^{14}N/^{15}N$ isotopic ratios in HCN and CH_3CN.

We now compare our derived scaled nitrogen isotopic ratio with the models of Vuitton et al. (2019) and Dobrijevic & Loison (2018) to gain better insight into how ^{15}N may be incorporated into CH_3CN. At the value of our peak observed altitudinal sensitivity ($\approx$ 230 km), our value of $^{14}N/^{15}N = 69 \pm 4$ is in better agreement with the Vuitton et al. (2019) model value of $\sim$55 than the Dobrijevic & Loison (2018) model (with GCRs) value of $\sim$120. A major difference between the models is in their treatment of the importance of magnetospheric electrons, which provide an additional source of atomic nitrogen, particularly important in the middle atmosphere (at altitudes 700-1200 km). Since electron-impact dissociation of N_2 is not isotope-selective, the resulting additional source of atomic nitrogen in this altitude range has a $^{14}N/^{15}N$ ratio equal to that of N_2. This causes the total atomic $^{14}N/^{15}N$ ratio to tend towards larger values, with a corresponding impact on the $^{14}N/^{15}N$ ratio for nitriles produced in this region. Our result suggests that the significance of dissociation of N_2 by energetic processing may need to be revisited. This implication is continued when the photochemical models are also compared to a continuously derived $^{14}N/^{15}N$ profile, as the continuous profile falls into a similar agreement with the models (see Appendix C).

While our derived isotopic ratios are in good agreement with previous measurements on Titan, it is of interest to compare with other Solar System bodies. Based on the data collated by Nomura et al. (2022)(and references therein), we identify some general trends for the $^{12}C/^{13}C$ and $^{14}N/^{15}N$ isotopic ratios. The carbon ratios are shown to have only small variations from planet to planet and most of the error bars are fairly well constrained. However, some measurements do have errors too large to constrain the exact variations. Most of the measurements for comets also maintain small variations, with the exception of the value of 40 $\pm$ 14 (Altwegg et al. 2020) for H_2CO in comet 67P, while some have large error bars that are also unable to completely constrain the variations. Meteorites have a larger range of variation. In contrast, the nitrogen isotopic ratios are shown to generally vary amongst the objects in the solar system and may have some smaller variations amongst

ratios of the same object depending on the molecule of interest.

Given the results of our study, we can speculate about the origin of Titan's dense nitrogen reservoir. In future studies, it would be useful to gain more insight into the the amount of N_2 that Titan has lost since it formed; the present-day isotopic ratios of heavy, noble gases would also be useful in this regard. This could help determine if Titan's N_2 was formed internally through hydrothermal and cryovolcanic processes or if the N_2 was formed through photochemical reactions involving accreted cometary ices. All the nitriles observed to date show a strong ^{15}N enrichment. As they mix downward, these nitriles condense into aerosols and precipitate onto the surface, so over time, some of the ^{15}N is removed from the atmosphere. Therefore, the overall atmospheric $^{14}N/^{15}N$ ratio should increase over time, suggesting that Titan's atmospheric nitrogen could have been more ^{15}N rich in the past — possibly more similar to the value of ≈ 144 found in comets (Nomura et al. 2022). To confirm this hypothesis will require continued, high-accuracy studies of $^{14}N/^{15}N$ ratios in cometary nitrogen-bearing species (N_2, NH_3, HCN and other organics), as well as in the various nitrogen-bearing compounds found in Titan's surface and atmosphere.

6. CONCLUSIONS

Using high signal-to-noise ALMA observations from 2019, we derived the first well-constrained isotopologue abundance ratios for CH_3CN in Titan's atmosphere: 68.9 ± 4.2 for $CH_3CN/CH_3C^{15}N$, 89.2 ± 7.0 for $CH_3CN/^{13}CH_3CN$, and 91.2 ± 6.0 for $CH_3CN/CH_3{}^{13}CN$. These ratios represent disk-averaged values, but are most sensitive to gases in the altitude range 150-300 km, with a peak sensitivity around 230 km. We therefore show for the first time that ^{15}N is strongly enhanced in CH_3CN compared to Titan's main atmospheric nitrogen reservoir (N_2). This can be explained as a result of photochemical isotopic fractionation initiated by isotope-selective photodissociation of N_2 in the thermosphere. We find a consistent level of ^{15}N enrichment within all Titan's nitriles measured to-date, which implies they likely formed from a common, isotopically fractionated reservoir of atmospheric nitrogen. Comparison between our scaled nitrogen isotopic ratio and the profiles from previous photochemical models shows that there is better agreement with the Vuitton et al. (2019) model. Using a continuous retrieval of the $CH_3C^{15}N$ abundance as a function of altitude, we derived a $^{14}N/^{15}N$ vertical profile that yields the same agreement with the photochemical models - there is better agreement with the Vuitton et al. (2019) model but the size of the 1-σ errors means agreement with either model cannot be ruled out.

This paper makes use of the following ALMA data: ADS/JAO.ALMA#2019.1.00783.S. ALMA is a partnership of ESO (representing its member states), NSF (USA) and NINS (JAPAN), together with NRC (Canada), NSTC and ASIAA (Taiwan), and KASI (republic of Korea), in cooperation with the Republic of Chile. The Joint ALMA Observatory is operated by ESO, AUI/NRAO, and NAOJ.

The work done by MAC, AET, and CAN was funded by NASA's Solar System Observation (SSO) Program, and this work was funded by the ALMA SOS program.

APPENDIX

A. CH_3CN SPECTROSCOPIC PARAMETERS AND PARTITION FUNCTIONS

We used frequency predictions of acetonitrile (methyl cyanide; CH_3CN) taken from the CDMS database (Müller et al. 2001) and noticed that the current CDMS predictions (Müller, H. S. P. et al. 2009) for the ground state were based on data with a significant missing window in experimental coverage around 257 GHz of current detections. The nearest experimental measurements were for the J=8-7 transition near 147 GHz (Boucher et al. 1977) and then the J=18-17 transition near 331 GHz (Cazzoli & Puzzarini 2006). For this reason we carried out an experimental double check of the prediction accuracy in this missing window, by measuring K=0 to 9 transitions for J=14-13 at 257 GHz and J=15-14 at 275 GHz. Measurements were made at room temperature, and at around 1 mTorr sample pressure by using the broadband millimeter-wave (MMW) spectrometer in Warsaw (Medvedev et al. 2004). This verification turned out to be positive since CDMS predictions and currently measured frequencies for 20 different transitions were in agreement to a root mean square deviation of 16 kHz, which is well within the nominal uncertainty of the employed spectrometer.

Table 2. Partition functions for CH_3CN isotopologues as a function of temperature

T (K)	Q(CH_3CN)	Q($^{13}CH_3CN$)	Q($CH_3{}^{13}CN$)	Q($CH_3C^{15}N$)
300.0	10118.2635	10418.8811	10123.2613	10431.9556
225.0	6570.5621	6765.7543	6573.8080	6774.2565
150.0	3576.3518	3682.5661	3578.1185	3687.1996
75.00	1265.1853	1302.7260	1265.8098	1304.3662
37.50	449.0803	462.3803	449.3016	462.9618
18.75	164.3168	169.1645	164.3975	169.3765
9.375	64.0955	65.9716	64.1267	66.0537

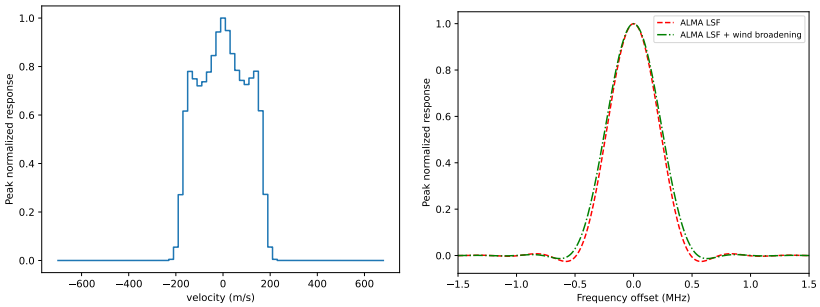

Figure 5. Spectral line broadening profile based on the CH_3CN wind field observed by Cordiner et al. (2020) (left), and final line spread function with wind induced broadening as well as the Hanning-smoothed sinc response of the ALMA correlator (right).

Another issue that we faced in deriving the isotopic ratios was the need for a unified partition function for the parent species and its ^{13}C isotopic variants. The values in the ground state entry in CDMS also accounted for the levels in the v_8=1 excited vibrational state, while those for the ^{13}C species did not. For this reason we re-evaluated the partition function for the ground state of the parent at the same conditions as for the isotopic species, namely without the v_8=1 state, and without accounting for the nitrogen hyperfine structure, which is unresolved at the resolution of our data. Omission of the CH_3CN vibrationally excited state amounts to a 7% underestimation of the partition function. As a result of these improvements to the line intensities and partition functions, we found that the retrieved isotopic ratios decreased by 20% for the $^{14}N/^{15}N$ ratio, 23% for the $CH_3CN/^{13}CH_3CN$ ratio and 27% for the $CH_3CN/CH_3{}^{13}CN$ ratio.

B. LINE SHAPE FUNCTION

In order to account for the potential effects of rotational broadening of the lines in the data, we generated a new instrumental line spread function for inclusion in NEMESIS. A rotationally broadened spectral profile was created using a modified version of the code published in Cordiner et al. (2020), including the impact of Titan's winds on the CH_3CN Doppler line profile based on the observed wind field in May 2017. We convolved the rotationally broadened profile with a line-shape function that mimics the ALMA correlator response, which is the Fourier transform of a (padded) Hann window, to get the new line spread function (Hunter 2016). Note the amount of padding used sets the frequency domain sampling and we set this to correspond to two channels, according to the standard setup of the ALMA correlator. Our observations were obtained at two different spectral resolutions (488 and 976 kHz), corresponding to a velocity FWHM of 568 and 1090 $m\,s^{-1}$ at 257.4461 and 267.5854 GHz, respectively. After the addition of wind broadening, the 488 kHz velocity FWHM increased to 604 $m\,s^{-1}$ (a difference of 36 $m\,s^{-1}$), and the 976 kHz velocity FWHM increased to 1109 $m\,s^{-1}$ (a difference of 19 $m\,s^{-1}$) so the LSF had a slight impact on the results.

C. CONTINUOUS $^{14}N/^{15}N$ PROFILE

When compared to the photochemical models, we find that our retrieved $^{14}N/^{15}N$ ratio continuous profile (Figure 1) is in better agreement with the Vuitton et al. (2019) model than the Dobrijevic & Loison (2018) model. However, upon removal of cosmic ray-induced chemistry, the Dobrijevic & Loison (2018) model provides a better match, although

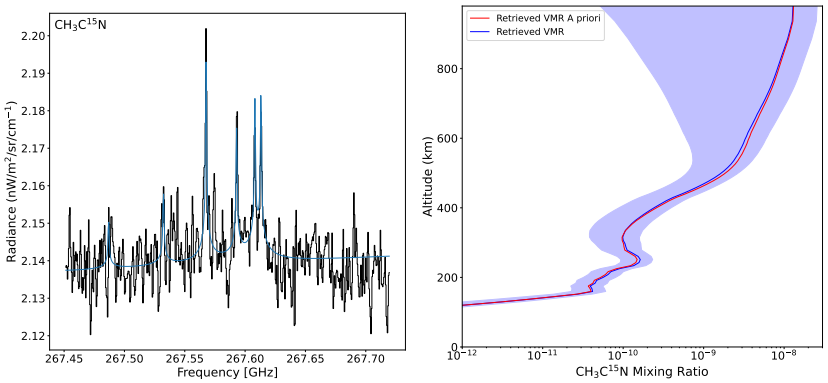

Figure 6. Continuously retrieved $CH_3C^{15}N$ model fit (left) and VMR profile (right). As in 1(a) and 1(b), the data is in black and the model in blue and in the right panel the red line is the a priori profile, the blue line is the retrieved VMR profile and the shaded region is error on the retrieved VMR profile. The χ^2_R for the model is 0.9386 which is an increase of 6e−4 over the scaling factor retrieval which is within a 1-σ difference and was calculated in the same manner as that described for Figure 1.

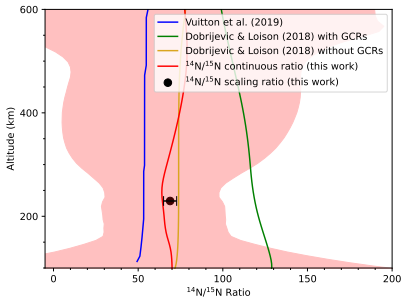

Figure 7. Derived continuous $CH_3CN/CH_3C^{15}N$ isotopic ratio profile with error envelope (red; shaded red region) plotted with photochemical model profiles from Vuitton et al. (2019) (blue) and Dobrijevic & Loison (2018) (green and gold). The black point is our derived scaling factor for the $CH_3CN/CH_3C^{15}N$ isotopic ratio from this work plotted at the obtained weighted mean emission altitude of 229.6 km with its corresponding error bars.

it is unclear whether such a model would be physically accurate. Considering the size of the (1-σ) error bars, our continuous retrieval provides a reasonably good match with Vuitton et al. (2019). The error envelope in the Figure represents the retrieval error, which denotes the region of highest sensitivity (smallest errors), and accounts for both the model and a-priori errors. Since the errors are so large, there is no strong evidence for variability in the $^{14}N/^{15}N$ ratio with altitude. The chi-square value also minimally changes from the scaling factor retrieval value of 376.1675 to the continuous retrieval value of 376.3835 (a difference of 0.2160) which falls within a 1-σ difference and means there is no significant improvement in the fit of the continuous retrieval. As discussed in section 5, the two photochemical models differ in the weight they give to the impact of magnetospheric electrons and so further investigations of $^{14}N/^{15}N$ as a function of altitude would be useful to help distinguish between the differing altitudinal dependencies of the two models as well as the impacts of the GCR chemistry, as this will impact the abundance (and thus isotope) profiles differently at different altitudes.

REFERENCES

Altwegg, K., Balsiger, H., Hänni, N., et al. 2020, Nature Astronomy, 4, 533, doi: 10.1038/s41550-019-0991-9

Balucani, N., Skouteris, D., Leonori, F., et al. 2012, The Journal of Physical Chemistry A, 116, 10467, doi: 10.1021/jp3072316

Boucher, D., Burie, J., Demaison, J., et al. 1977, Journal of Molecular Spectroscopy, 64, 290, doi: https://doi.org/10.1016/0022-2852(77)90267-3

Cazzoli, G., & Puzzarini, C. 2006, Journal of Molecular Spectroscopy, 240, 153, doi: https://doi.org/10.1016/j.jms.2006.09.013

Cordiner, M. A., Garcia-Berrios, E., Cosentino, R. G., et al. 2020, The Astrophysical Journal Letters, 904, L12, doi: 10.3847/2041-8213/abc688

Cordiner, M. A., Nixon, C. A., Charnley, S. B., et al. 2018, The Astrophysical Journal Letters, 859, L15, doi: 10.3847/2041-8213/aac38d

Cordiner, M. A., Teanby, N. A., Nixon, C. A., et al. 2019, The Astronomical Journal, 158, 76, doi: 10.3847/1538-3881/ab2d20

Cordiner, M. A., Palmer, M. Y., Nixon, C. A., et al. 2015, The Astrophysical Journal Letters, 800, L14, doi: 10.1088/2041-8205/800/1/L14

Dobrijevic, M., & Loison, J. 2018, Icarus, 307, 371, doi: https://doi.org/10.1016/j.icarus.2017.10.027

Dudaryonok, A., Lavrentieva, N., & Buldyreva, J. 2015, Icarus, 250, 76, doi: https://doi.org/10.1016/j.icarus.2014.11.020

Glein, C. R. 2015, Icarus, 250, 570, doi: https://doi.org/10.1016/j.icarus.2015.01.001

Hunter, T. 2016, Note on Spectral Response, Tech. rep.

Hörst, S. M. 2017, Journal of Geophysical Research: Planets, 122, 432, doi: https://doi.org/10.1002/2016JE005240

Iino, T., Sagawa, H., & Tsukagoshi, T. 2020, The Astrophysical Journal, 890, 95, doi: 10.3847/1538-4357/ab66b0

Irwin, P., Teanby, N., de Kok, R., et al. 2008, Journal of Quantitative Spectroscopy and Radiative Transfer, 109, 1136, doi: https://doi.org/10.1016/j.jqsrt.2007.11.006

Jennings, D. E., Nixon, C. A., Jolly, A., et al. 2008, The Astrophysical Journal, 681, L109, doi: 10.1086/590534

Jolly, A., Fayt, A., Benilan, Y., et al. 2010, ApJ, 714, 852, doi: 10.1088/0004-637X/714/1/852

Lellouch, E., Gurwell, M. A., Moreno, R., et al. 2019, An intense thermospheric jet on Titan. https://arxiv.org/abs/1903.12116

Liang, M.-C., Heays, A. N., Lewis, B. R., Gibson, S. T., & Yung, Y. L. 2007, The Astrophysical Journal, 664, L115, doi: 10.1086/520881

Loison, J., Hébrard, E., Dobrijevic, M., et al. 2015, Icarus, 247, 218, doi: https://doi.org/10.1016/j.icarus.2014.09.039

MacKenzie, S. M., Birch, S. P. D., Hörst, S., et al. 2021, The Planetary Science Journal, 2, 112, doi: 10.3847/PSJ/abf7c9

Mandt, K. E., Mousis, O., Lunine, J., & Gautier, D. 2014, The Astrophysical Journal Letters, 788, L24, doi: 10.1088/2041-8205/788/2/L24

Marten, A., Hidayat, T., Biraud, Y., & Moreno, R. 2002, Icarus, 158, 532, doi: https://doi.org/10.1006/icar.2002.6897

Medvedev, I., Winnewisser, M., De Lucia, F. C., et al. 2004, Journal of Molecular Spectroscopy, 228, 314, doi: https://doi.org/10.1016/j.jms.2004.06.011

Molter, E. M., Nixon, C. A., Cordiner, M. A., et al. 2016, The Astronomical Journal, 152, 42, doi: 10.3847/0004-6256/152/2/42

Müller, H. S. P., Thorwirth, S., Roth, D. A., & Winnewisser, G. 2001, A&A, 370, L49, doi: 10.1051/0004-6361:20010367

Müller, H. S. P., Drouin, B. J., & Pearson, J. C. 2009, AA, 506, 1487, doi: 10.1051/0004-6361/200912932

Niemann, H. B., Atreya, S. K., Demick, J. E., et al. 2010, Journal of Geophysical Research: Planets, 115, doi: https://doi.org/10.1029/2010JE003659

Nixon, C., Achterberg, R., Vinatier, S., et al. 2008a, Icarus, 195, 778, doi: https://doi.org/10.1016/j.icarus.2008.01.012

Nixon, C., Lorenz, R., Achterberg, R., et al. 2018, Planetary and Space Science, 155, 50, doi: https://doi.org/10.1016/j.pss.2018.02.009

Nixon, C. A. 2024, ACS Earth and Space Chemistry, 8, 406–456, doi: 10.1021/acsearthspacechem.2c00041

Nixon, C. A., Jennings, D. E., Bézard, B., et al. 2008b, The Astrophysical Journal, 681, L101, doi: 10.1086/590553

Nixon, C. A., Thelen, A. E., Cordiner, M. A., et al. 2020, The Astronomical Journal, 160, 205, doi: 10.3847/1538-3881/abb679

Nomura, H., Furuya, K., Cordiner, M., et al. 2022. https://arxiv.org/abs/2203.10863

Oro, J., Miller, S. L., & Lazcano, A. 1990, Annual Review of Earth and Planetary Sciences, 18, 317, doi: https://doi.org/10.1146/annurev.ea.18.050190.001533

Palmer, M. Y., Cordiner, M. A., Nixon, C. A., et al. 2017, Science Advances, 3, e1700022, doi: 10.1126/sciadv.1700022

Serigano, J., Nixon, C. A., Cordiner, M. A., et al. 2016, The Astrophysical Journal Letters, 821, L8, doi: 10.3847/2041-8205/821/1/L8

Teanby, N., Irwin, P., Nixon, C., et al. 2013, Planetary and Space Science, 75, 136, doi: https://doi.org/10.1016/j.pss.2012.11.008

Teanby, N. A., Sylvestre, M., Sharkey, J., et al. 2019, Geophysical Research Letters, 46, 3079, doi: https://doi.org/10.1029/2018GL081401

Teanby, N. A., de Kok, R., Irwin, P. G. J., et al. 2008, Journal of Geophysical Research: Planets, 113, doi: https://doi.org/10.1029/2008JE003218

Teanby, N. A., Bézard, B., Vinatier, S., et al. 2017, Nature Communications, 8, 1586, doi: 10.1038/s41467-017-01839-z

Thelen, A. E., Nixon, C., Chanover, N., et al. 2019, Icarus, 319, 417, doi: https://doi.org/10.1016/j.icarus.2018.09.023

Thelen, A. E., Cordiner, M. A., Nixon, C. A., et al. 2020, The Astrophysical Journal Letters, 903, L22, doi: 10.3847/2041-8213/abc1e1

Thelen, A. E., Nixon, C. A., Cordiner, M. A., et al. 2024, The Planetary Science Journal, 5, 125, doi: 10.3847/PSJ/ad47bd

Vinatier, S., Bézard, B., & Nixon, C. A. 2007, Icarus, 191, 712, doi: 10.1016/j.icarus.2007.06.001

Vuitton, V., Yelle, R., Klippenstein, S., Hörst, S., & Lavvas, P. 2019, Icarus, 324, 120, doi: https://doi.org/10.1016/j.icarus.2018.06.013

Willacy, K., Allen, M., & Yung, Y. 2016, The Astrophysical Journal, 829, 79, doi: 10.3847/0004-637x/829/2/79

Wilson, E. H., & Atreya, S. K. 2004, Journal of Geophysical Research: Planets, 109, doi: https://doi.org/10.1029/2003JE002181